CHEMISTRY
A EUROPEAN JOURNAL

DOI: 10.1002/chem.200600529

Methyl Vinyl Ketone + OH and Methacrolein + OH Oxidation Reactions: A Master Equation Analysis of the Pressure- and Temperature-Dependent Rate Constants

Montserrat Ochando-Pardo,[b] Ignacio Nebot-Gil,[b] Àngels González-Lafont,*[a] and José M. Lluch[a]

Abstract: High-level electronic structure calculations and master equation analyses were carried out to obtain the pressure- and temperature-dependent rate constants of the methyl vinyl ketone + OH and methacrolein + OH reactions. The balance between the OH addition reactions at the high-pressure limit, the OH addition reactions in the fall-off region, and the pressure-independent hydrogen abstractions involved in these multiwell and multichannel systems, has been shown to be crucial to understand the pressure and temperature dependence of each global reaction. In particular, the fall-off region of the OH addition reactions contributes to the inverse temperature dependence of the rate constants in the Arrhenius plots, leading to pressure-dependent negative activation energies. The pressure dependence of the methyl vinyl ketone + OH reaction is clearly more important than in the case of the methacrolein + OH reaction owing to the weight of the hydrogen abstraction process in this second system. Comparison of the theoretical rate constants and the experimental measurements shows quite good agreement.

Keywords: gas-phase reactions · kinetics · master equation · methacrolein · methyl vinyl ketone · oxidation

Introduction

Atmospheric chemistry has received a great deal of attention in recent decades.[1,2] It is now clear that both human-induced and biogenic emissions can significantly influence the Earth's atmosphere. Understanding the fate of atmospheric pollutants and the chemical processes they undergo is key for modeling and predicting atmospheric changes, such as ozone depletion and production, the long-range transport and transformation of toxic substances, regional air quality alteration, or global climate changes.[3,4]

Progress in this field has been made possible by improvements in both the experimental techniques and the theoretical methods that are employed to determine the rate constants of the reactions that occur in the Earth's atmosphere. From the theoretical side quite elaborated variants of transition-state theory are well established.[5,6] Their huge power and efficiency in providing reliable estimations of gas-phase rate constants that depend just on the temperature (that is, independent of pressure, as in complex reactions occurring at their high-pressure limit) have been widely recognized for a long time. However, many reactions are both temperature- and pressure-dependent. So, because the Earth's atmosphere has an enormous range of pressure and temperature conditions, pressure-dependent reactions are found at virtually all altitudes from the surface to well over 100 km.[3,4]

When the rate of collisional energy transfer (which depends on the total pressure) is competitive with the rate of a reactive chemical process that depends on internal energy, the overall reaction is pressure-dependent.[7,8] Association bimolecular reactions (which are frequently encountered in atmospheric chemistry), leading to highly vibrationally excited intermediates that are capable of further unimolecular dissociation, isomerization, or collisional stabilization, are a clear example of this kind of reaction. Master equations, giving the continuous-time evolution of a probability distribution, are then required to accurately describe the simultaneous interplay of collisional energy transfer and chemical

[a] Dr. À. González-Lafont, Prof. Dr. J. M. Lluch
Universitat Autònoma de Barcelona, Departament de Química
08193 Bellaterra, Barcelona (Spain)
Fax: (+34) 93-581-2920
E-mail: angels@klingon.uab.es

[b] Dr. M. Ochando-Pardo, Prof. Dr. I. Nebot-Gil
Universitat de València, Institut de Ciència Molecular
Apdo. 22085, 46071 València (Spain)

Supporting information for this article is available on the WWW under http://www.chemeurj.org/ or from the author.

WILEY InterScience DISCOVER SOMETHING GREAT
© 2007 Wiley-VCH Verlag GmbH & Co. KGaA, Weinheim

reactions.[8] With the recent development of several methods and efficient software packages for solving the master equations, the strength of the theoretical methods providing reliable rate constants and detailed pictures of the mechanism of pressure-dependent atmospheric reactions is approaching that of pressure-independent reactions.[7,9–12]

In this work we have combined high-level electronic structure calculations, Rice–Ramsperger–Kassel–Marcus (RRKM)[13] theory, and the MultiWell computer program suite[7] to solve the one-dimensional master equation, to shed light on the subtle balance between the different channels involved in the methyl vinyl ketone (MVK)+OH and methacrolein (MACR)+OH oxidation reactions, and to determine their corresponding overall rate constants under a wide range of temperature–pressure experimental conditions. As will be seen below, the good agreement of our results with experimental measurements in these specially challenging cases shows that the theoretical study of pressure-dependent reactions is becoming a mature field.

MVK (3-buten-2-one) and MACR (2-methyl-2-propenal) are two of isoprene's major oxidation byproducts. Isoprene is the most abundant non-methane hydrocarbon emitted into the troposphere.[3,4] Isoprene, MVK, and MACR have an important role in ozone production. The dominant process by which both MVK and MACR are removed from the atmosphere is through reaction with the OH radical, the most important daytime oxidant in the troposphere. These reactions are two striking examples in which pressure determines the subtle balance between different processes. The OH radical reacts with MVK at the terminal and central carbon atoms of the double bond to form addition products [reaction (R1), in which M stands for a third body], with an experimental branching ratio for the reaction pathway R1t of at least 70% at atmospheric pressure and 298 K.[14a]

$$CH_2{=}CHC(O)CH_3 + OH + M \rightarrow CH_2(OH)CHC(O)CH_3 + M \quad \text{(R1t)}$$

$$CH_2{=}CHC(O)CH_3 + OH + M \rightarrow CH_2CH(OH)C(O)CH_3 + M \quad \text{(R1c)}$$

On the other hand, the MACR+OH system [reaction (R2)] can undergo terminal and central OH additions or an abstraction of the aldehydic hydrogen atom by OH, with experimental branching ratios of 50:50[14b] or 55:45[3] for the OH additions versus the hydrogen atom abstraction, and of at least 85% for the addition of OH to the terminal carbon atom in comparison with the addition to the central carbon atom at room temperature and atmospheric pressure.

$$CH_2{=}C(CH_3)CHO + OH + M \rightarrow CH_2(OH)C(CH_3)CHO + M \quad \text{(R2t)}$$

$$CH_2{=}C(CH_3)CHO + OH + M \rightarrow CH_2C(OH)(CH_3)CHO + M \quad \text{(R2c)}$$

$$CH_2{=}C(CH_3)CHO + OH \rightarrow CH_2{=}C(CH_3)CO + H_2O \quad \text{(R2H)}$$

Until very recently, no pressure dependence had been observed for the overall R1 and R2 reactions. The corresponding rate constants (2.03×10^{-11} and 2.79×10^{-11} $cm^3 molecule^{-1} s^{-1}$ for MVK and MACR, respectively, at 298 K),[15] measured over the temperature range 232–378 K using the pulsed laser photolysis/pulsed-laser-induced fluorescence technique, were found to be independent of pressure in the range of 20–300 torr by Ravishankara and co-workers. However, Chuong and Stevens,[16] using the discharge-flow technique coupled with laser-induced fluorescence and resonance fluorescence detection of the OH radical, found that the rate constant for the overall MVK+OH reaction is dependent on pressure between 2–5 torr in the range 328–422 K, although no pressure dependence was found at 300 K (the measured rate constant was found to be $(1.73\pm0.21)\times10^{-11}$ $cm^3 molecule^{-1} s^{-1}$ at 5 torr and 300 K). These results suggest that the MVK+OH reaction is dominated by the OH addition process, which is pressure-dependent, the system being near its high-pressure limit (the rate constant is independent of pressure) at room temperature, but in its fall-off region (the rate constant decreases as the pressure falls) at higher temperatures. This behavior is due to the shift of the fall-off region to higher pressures as the temperature rises. In contrast, in the same study, the overall MACR+OH reaction did not show any significant dependence on pressure at 2–5 torr in the range 300–422 K. These results now suggest that over the range of pressures and temperatures studied the aldehydic hydrogen-abstraction process dominates over the OH addition reactions. The measured rate constant was found to be $(3.23\pm0.36)\times10^{-11}$ $cm^3 molecule^{-1} s^{-1}$ at 2 torr and 300 K.

Later, Chuong and Stevens[17] examined these two reactions at higher pressures using a turbulent flow technique coupled with laser-induced fluorescence detection of the OH radical. The overall rate constants for the MVK and MACR reactions were measured to be $(1.78\pm0.08)\times10^{-11}$ and $(3.22\pm0.10)\times10^{-11}$ $cm^3 molecule^{-1} s^{-1}$, respectively, at 100 torr and 300 K, this way confirming that both reactions are pressure-independent at room temperature. In turn, Sidebottom and co-workers,[18] using a pulsed laser photolysis/laser-induced fluorescence technique, obtained a value of $(1.86\pm0.12)\times10^{-11}$ $cm^3 molecule^{-1} s^{-1}$ for the overall MVK reaction at 298 ± 2 K and atmospheric pressure.

The linear Arrhenius plots fitted by Chuong and Stevens[16] for these two reactions show the pressure effect to be even more interesting. The plot for the overall MVK+OH reaction exhibits a negative temperature dependence ($E_a/R=-(1170\pm80)$ K) in the range 300–422 K at 5 torr, and this value is more negative than those obtained by Kleindienst et al. ($E_a/R=-(456\pm73)$ K) between 298 and 424 K

 © 2007 Wiley-VCH Verlag GmbH & Co. KGaA, Weinheim

at 50 torr,[19] and Gierczak et al. ($E_a/R = -(612\pm49)$ K) between 232 and 378 K at 16–100 torr.[15]

Much more surprising is the dependence of the activation energy of the overall MACR + OH reaction on the pressure (it has to be remembered that, as mentioned above, no significant pressure dependence had been observed for this reaction between 2 and 5 torr within the range 300–422 K), as the same pattern as in the MVK + OH system is obtained. Again, a negative temperature dependence ($E_a/R = -(1050\pm120)$ K) in the Arrhenius plot between 300 and 422 K at 5 torr was found by Chuong and Stevens[16] for the overall MACR + OH reaction. This negative temperature dependence turned out to be more negative than that measured by Kleindienst et al. ($E_a/R = -(175\pm52)$ K) between 300 and 423 K at 50 torr,[19] and by Gierczak et al. ($E_a/R = -(379\pm46)$ K) between 234 and 373 K at 20–100 torr.[15]

Previously[20] we carried out high-level electronic structure calculations, exploring the potential-energy surfaces of the addition and hydrogen-abstraction reactions involved in the overall R1 and R2 reactions. To our knowledge, that was the first time that these reactions had been studied theoretically, at least using high-level ab initio methods. The results allowed us to identify some key features of the potential-energy surfaces that are very important for gaining an insight into the basis of the pressure dependence. Indeed a proper study and understanding of these quite challenging reactions require dynamic calculations and the determination of rate constants that can be compared directly with experimental measurements. This was the aim of the work reported in this paper, in which additional electronic structure calculations are also presented.

Computational Methods

Electronic structure calculations: All the stationary points were optimized by using hybrid density functional theory (HDFT) with the MPW1K functional[21] and the 6-31 + G(d,p) basis set. The nature of the stationary points was characterized by analyzing the eigenvalues of the Hessian matrices in mass-weighted Cartesian coordinates at the same level of electronic structure calculations. A scale factor of 0.9515[22] was applied to the zero-point energy (ZPE).

In the case of the terminal OH additions to the antiperiplanar conformers of MVK and MACR, the MPW1K/6-31 + G(d,p) saddle points turned out to be too loose (the C−O distances are 3.1 and 3.2 Å, respectively). Because these kinds of generalized gradient functionals do not treat dispersion forces explicitly, they often fail to describe long-range weak interactions.[23,24] We can then guess that these two loose transition-state structures would be inappropriate to use to correctly obtain the rate constants. To circumvent this problem, the MP2/6-31 + G(d,p) stationary points involved in these two terminal OH additions were optimized and characterized. On the other hand, it has been proved that the MP2 vibrational frequencies often suffer from spin contamination.[25] So, once these additions had been characterized, MPW1K/6-31 + G(d,p) frequency calculations using the MP2/6-31 + G(d,p) geometries corrected with the RODS algorithm[26,27] were performed with the aim of improving the vibrational frequency description. The same scale factor as the one used for the rest of the stationary points (0.9515) was applied to the ZPE. We determined the minima associated with each transition-state structure by constructing the corresponding minimum energy path (MEP).

Single-point energy calculations on all the MPW1K/6-31 + G(d,p) and MP2/6-31 + G(d,p) stationary-point geometries were performed at the CCSD(T)/cc-pVTZ level in order to obtain higher level energies and to overcome the spin contamination problem found at some of the stationary points.[28,29] Nowadays, there is some discussion as to whether open-shell systems suffering from spin contamination are better described by the restricted or unrestricted formalism of the coupled cluster method. In order to choose, several trials with both the restricted (RCC) and the unrestricted (UCC) coupled cluster method, using either a restricted (RHF) or an unrestricted (UHF) Hartree–Fock reference wave function, were performed. Specifically, the UHF-UCCSD(T), RHF-UCCSD(T), and RHF-RCCSD(T)[30–33a] methods were tested and the results for one of the systems studied are shown in Table 1. It can be observed that the classical potential-energy barriers are very similar (the difference is less than 0.5 kcal mol^{-1}), in accordance with Chuang et al.[28] The UHF-UCCSD(T) method was chosen to perform the calculations on all the open-shell molecules of the potential-energy surface. So, unless specified otherwise, we always refer to the unrestricted formalism when we talk about the CCSD(T) method.

Table 1. Classical potential-energy barriers [kcal mol^{-1}] obtained from single-point CCSD(T)/cc-pVDZ energy calculations on the MACR + OH saddle points.

	RHF-RCCSD(T)	RHF-UCCSD(T)	UHF-UCCSD(T)
TSadd-t-*ap2*[a]	−1.47	−1.18	−1.18
TSadd-c-*ap2*[b]	0.80	0.36	0.70
TSabs-*ap2*[b]	0.75	0.35	0.36

[a] Located at the MP2/6-31 + G(d,p) level. [b] Located at the MPW1K/6-31 + G(d,p) level.

The basis set correction approach recommended by Lei et al. for the study of atmospheric reactions of volatile organic compounds (VOCs) was applied.[33b] It involves a projected Møller–Plesset calculation (PMP2) using both cc-pVTZ and cc-pVQZ basis sets, and the final result approximates to a CCSD(T)/cc-pVQZ level calculation. Thus, in this paper, the acronym CCSD(T)/cc-pVTZ(Q) represents electronic structure calculations that include the basis set correction approach.

Except for the tests on open-shell molecules using the RHF-UCCSD(T) and RHF-RCCSD(T) methods, restricted and unrestricted spin formalisms were used on closed and open-shell molecules, respectively.

The Gaussian 03 package[34] was used for all the electronic structure calculations except for the tests with RHF-UCCSD(T) and RHF-RCCSD(T) on open-shell molecules, which were carried out using the MOLPRO[35] program.

Master equation calculations: A reaction becomes pressure-dependent when the rate of collisional energy transfer competes with the rate of a chemical process that depends on internal energy.[7] In this work, we can distinguish three different schemes for pressure-dependent reactions [reactions (S1), (S2), and (S3)].

$$A + B \rightleftharpoons AB^* \rightarrow AB \quad \text{(S1)}$$

$$\begin{array}{l} A + B \rightleftharpoons CD^* \rightarrow C + D \\ \qquad\quad \downarrow \\ \qquad\quad CD \end{array} \quad \text{(S2)}$$

$$\begin{array}{l} A + B \rightleftharpoons AB_1^* \rightleftharpoons AB_2^* \\ \qquad\quad \downarrow \qquad\ \downarrow \\ \qquad\quad AB_1 \quad\ AB_2 \end{array} \quad \text{(S3)}$$

The simpler case, reaction (S1), corresponds to an addition reaction in which the vibrationally excited adduct AB* can revert to reactants or be collisionally stabilized, both processes being competitive. A more complex scheme is illustrated in reaction (S2); an excited product complex is

 © 2007 Wiley-VCH Verlag GmbH & Co. KGaA, Weinheim

formed, CD*, which can revert to reactants, be collisionally stabilized, or undergo irreversible dissociation. Finally, in reaction (S3), an initial excited adduct, AB_1*, is formed which can revert to the reactants, be collisionally stabilized, or reversibly isomerize to a second excited adduct, AB_2*, which can revert to the excited AB_1* adduct or be collisionally stabilized. For each of these reactive schemes, the population of the species formed in the mechanism depends on the pressure. For all the pathways considered in this work the initial transition-state structure lies below the corresponding reactants and is preceded by a hydrogen-bonded complex. In all cases, the well of this complex is not very deep in terms of adiabatic potential energy (classical potential energy plus ZPE), and disappears in terms of Gibbs free energy at or above 300 K. As a consequence, these complexes have not been taken into account in the master equation calculations.

At sufficiently high pressures, the vibrationally excited intermediate species are stabilized by collisions with other molecules and the reaction rate constant becomes pressure-independent. In this case, a bimolecular recombination rate constant is related to the corresponding reverse unimolecular rate constant by Equation (1), in which K_{eq} is the recombination reaction equilibrium constant. Here, the equilibrium constants were calculated with the Thermo program included in the MultiWell package.[36]

$$k_{rec,\infty} = k_{uni,\infty} K_{eq} \tag{1}$$

On the other hand, at intermediate and low pressures, there is competition between the collisional and reactive processes. In these cases it is necessary to determine the populations of all the wells of the potential-energy surface at each pressure. The master equation provides a quantitative time-dependent description of the interplay of collisional energy transfer and chemical reactions in order to obtain those populations depending on pressure. The monodimensional, that is, internal-energy-dependent master equation can be written[37] as Equation (2), in which $y(E',t)\mathrm{d}E'$ is the concentration of species with internal energy in the range between E' and $E'+\mathrm{d}E'$, $R(E,E')$ is the pseudo-first-order rate constant for the internal energy transfer from energy E' to energy E, $f(E',t)\mathrm{d}E'$ is a source term (that is, the formation rate of a species with an internal energy between E' and $E'+\mathrm{d}E'$ from the incoming two reactants), and $k_i(E')$ is the unimolecular rate constant for the ith channel. The internal energy E is assumed to be fully randomized among the active degrees of freedom (vibrations and an active external rotation). Terms involving radiative emission and absorption have been omitted owing to their low efficiency.

$$\frac{\mathrm{d}y(E',t)}{\mathrm{d}t}\mathrm{d}E' = f(E',t)\mathrm{d}E' + \int_0^\infty [R(E',E)\mathrm{d}E' y(E,t)]\mathrm{d}E - \int_0^\infty [R(E,E')\mathrm{d}E' y(E',t)]\mathrm{d}E - \sum_{i=1}^{\text{channels}} k_i(E') y(E',t)\mathrm{d}E' \tag{2}$$

In this work, the MultiWell program suite[36,37] was used to solve the master equation by means of an adaptation of Gillespie's exact stochastic method. This program uses a hybrid master equation approach involving an energy-grained master equation at low vibrational energies and a continuum master equation in the quasicontinuum at high vibrational energies.[37] The source term of Equation (2) is not considered in the MultiWell package. Instead, the chemical activation energy distribution was chosen to describe the nascent energy distribution of the complex formed in the recombination of species A and B [reactions (S1)–(S3)].[38]

To calculate the overall rate constant for producing the ith product at intermediate and low pressures, the relative population f_i of the species at the end of the simulation (within the steady-state regime), that is, when the complexes that have not decomposed are collisionally thermalized in the wells, is multiplied by $k_{rec,\infty}$ [Equation (3)].

$$k = f_i k_{rec,\infty} = f_i k_{uni,\infty} K_{eq} \tag{3}$$

In Equation (2), the microcanonical rate constants, $k_i(E)$, for the unimolecular processes are calculated by applying Equation (4) to the saddle-point structure, where $G^{\ddagger}(E-E_0)$ is the sum of states of the transition state, E_0 is the reaction threshold energy, h is Planck's constant, and $\rho(E)$ is the density of the states of the reactant molecule. The internal energy E is measured relative to the zero-point energy of the reactant molecule. σ corresponds to the symmetry factor defined by Equation (5),[39] in which σ^R is the rotational symmetry number of the unimolecular reactant, $\sigma^{\ddagger}$(s) corresponds to the saddle point, and $n^{\ddagger}$ and n are the number of optical isomers of the saddle-point structure and unimolecular reactant, respectively. The magnitudes of $G^{\ddagger}(E-E_0)$ and $\rho(E)$ in Equation (4) correspond to a single optical isomer and so it is necessary to correct the equation by using the $n^{\ddagger}$ and n parameters. In this work, $n^{\ddagger}$ was considered to be 2 for all the saddle points except for the hydrogen abstraction of MACR (R2H), which has planar geometry and $n^{\ddagger}=1$, while n was considered to be 2 for all the unimolecular reactants. So, $\sigma=1$ for all the reactions except for the hydrogen abstraction of MACR (R2H), where a value of $^1/_2$ for σ was used.

$$k(E) = \sigma \frac{1}{h} \frac{G^{\ddagger}(E-E_0)}{\rho(E)} \tag{4}$$

$$\sigma = \frac{n^{\ddagger}\sigma^R}{n\sigma^{\ddagger}} \tag{5}$$

The scaled MPW1K/6-31+G(d,p) vibrational frequencies and the moments of inertia obtained with the Mominert program included in the MultiWell package[36] were used to calculate the densities and sums of states within the harmonic and rigid-rotor approximations. Calculations of the densities and the sums of states were performed by using the Stein–Rabinovitch[40] adaptation of the Beyer–Swinehart algorithm included in the Densum program[36] with an energy grain of 10 cm^{-1}.

The microcanonical rate constant $k(E)$ was also used to calculate the unimolecular rate constant at the high-pressure limit[37] with Equation (6), in which $Q(T)$ is the partition function of the internal degrees of freedom of the reactant at temperature T [Equation (7)].

$$k_{uni,\infty}(T) = \frac{1}{Q(T)} \int_{E_0}^{\infty} k(E)\rho(E)\exp(-E/k_B T)\mathrm{d}E \tag{6}$$

$$Q(T) = \int_0^{\infty} \rho(E)\exp(-E/k_B T)\mathrm{d}E \tag{7}$$

The total angular momentum, J, was not explicitly included in the calculation of the microcanonical rate constant, but the K rotor approximation was applied, for which one external rotation is considered active (corresponding to the smallest moment of inertia of the molecule), unlike the other two, which remain inactive. Centrifugal corrections at a given temperature for angular momentum conservation were applied to the threshold energy[41,42] [Equation (8), in which I_A and $I_A{}^{\ddagger}$ are the moments of inertia for the external two-dimensional inactive rotations of the reactant and transition state, respectively]. The Densum program included in the MultiWell package[36] was used to obtain the unimolecular rate constants $k(E)$.

$$E_0 = E_0^{\text{uncorrected}} - k_B T\left\{1 - \frac{I_A}{I_A{}^{\ddagger}}\right\} \tag{8}$$

The collisional energy transfer rate constant in the master equation, $R(E,E')$, was determined by calculation of the frequency of inelastic collisions, ω, and the choice of a collision step-size distribution, $P(E,E')$,[37] using Equation (9). The frequency of inelastic collisions was calculated from the Lennard-Jones parameters (Table 2), which were estimated from the critical properties of the molecule.[43–45] The critical properties were obtained from approximate empirical formulae, for which it is only necessary to know the number of bonds of each type in a molecule.[46] Helium was chosen as a collider gas. The collision step-size distribution selected herein is a generalized version of the exponential-down model[47]

 © 2007 Wiley-VCH Verlag GmbH & Co. KGaA, Weinheim

Table 2. Lennard-Jones parameters used for the MVK+OH and MACR+OH systems.

	σ_{LJ} [Å]	ε/k_B [K]
MVK	5.2	557
MACR	5.2	540

[Equation (10)]. In this model $N(E')$ is a normalization factor, α and γ are the energy transfer parameters from the toluene energy transfer properties measured by the kinetically controlled selective ionization (KCSI) method. The values, $\gamma = 0.7$ and $\alpha(E') = 43.5 + 0.0042E'$ (in cm^{-1}), are recommended by Barker et al. for non-"stiff" molecules.[37]

$$R(E,E')dE = \omega P(E,E')dE \quad (9)$$

$$P(E,E') = \frac{1}{N(E')}\exp\left[-\left(\frac{E'-E}{\alpha(E')}\right)^{\gamma}\right] \qquad \text{for } E' > E \quad (10)$$

An energy grain size of 10 cm^{-1} was used, whereas the maximum energy specified for the numerical solution of the master equation was 85000 cm^{-1}. To give a reasonable statistical error, 10^4 stochastic trials were tested. The master equation was solved in the temperature and pressure range of 298.15–425 K and 2–100 torr, respectively.

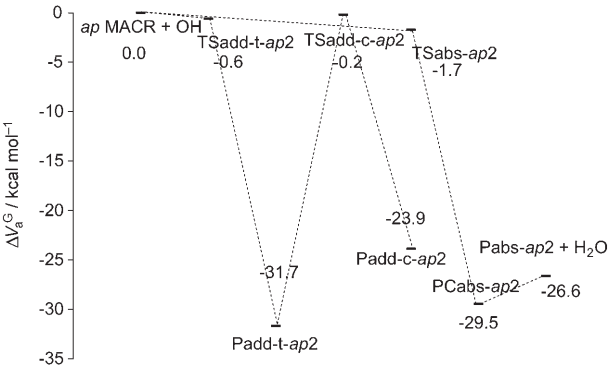

Figure 2. Potential-energy surface including the ZPE for the system MACR+OH at the CCSD(T)/cc-pVTZ(Q)//MPW1K/6-31+G(d,p) level of theory, except for the Padd-t-*ap*2 addition channel which was first calculated at the CCSD(T)/cc-pVTZ(Q)//MP2/6-31+G(d,p) level. Then the saddle-point energy of this latter addition reaction was lowered 1.5 kcal mol^{-1} (see text). The energies, which are relative to the *ap* MACR+OH energy, are expressed in kcal mol^{-1}. Pathways R2t (add-t), R2c (add-c), and R2H (abs) are represented with their corresponding transition-state structures (TS), product complex (PC), and products (P). Only the antiperiplanar (*ap*) conformer of MACR was considered.

Results

The potential-energy surfaces including the zero-point energy (adiabatic energy) for the MVK+OH and MACR+OH systems are shown in Figures 1 and 2, respectively, at the CCSD(T)/cc-pVTZ(Q)//MPW1K/6-31+G(d,p) level of theory (with the exception explained below). In both cases, only the main channels were taken into account. See ref. [20] for a complete electronic structure discussion of the whole potential-energy surface.

MVK+OH system: As can be observed in Figure 1, two conformers of the MVK molecule were taken into account. The two conformers arise as a result of an internal rotation around the C–C single bond joining the vinyl and the ketone moieties of the molecule. Depending on whether the C=O and C=C double bonds appear on the same or opposite side with respect to the C–C single bond, the conformer is described as synperiplanar (*sp*) or antiperiplanar (*ap*). The *ap* conformer was experimentally found to be more abundant at 300 K, with an *ap*:*sp* ratio of 80:20.[48] Our calculations at the CCSD(T)/cc-pVTZ(Q)//MPW1K/6-31+G(d,p) level give an *ap*:*sp* ratio that ranges from 61:39 at 298.15 K to 56:44 at 425 K. In view of this, the pathways of the MVK *sp* conformer were included in our analysis.

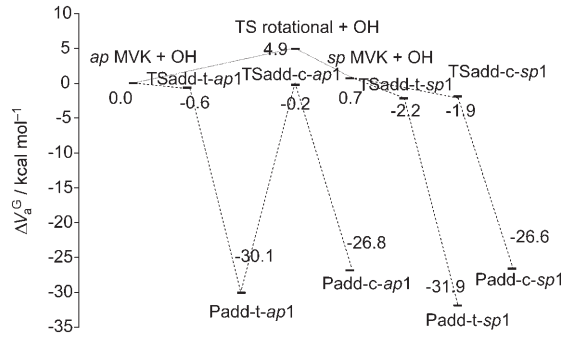

Figure 1. Potential-energy surface including the ZPE for the system MVK+OH at the CCSD(T)/cc-pVTZ(Q)//MPW1K/6-31+G(d,p) level of theory, except for the Padd-t-*ap*1 addition channel, which was first calculated at the CCSD(T)/cc-pVTZ(Q)//MP2/6-31+G(d,p) level. Then the saddle-point energy of this latter addition reaction was lowered 1.5 kcal mol^{-1} (see text). The energies, which are relative to the *ap* MVK+OH energy, are expressed in kcal mol^{-1}. Pathways R1t (add-t) and R1c (add-c) are represented along with their corresponding transition-state structures (TS) and products (P). Both the antiperiplanar (*ap*) and synperiplanar (*sp*) conformers of MVK were considered.

Determination of the location of the *ap* terminal addition transition-state structure, TSadd-t-*ap*1, is a challenge from an electronic structure point of view. The functional used [MPW1K/6-31+G(d,p)] provided a distance between the OH and MVK fragments that is too long (the C–O distance is 3.1 Å). As a consequence, a very low barrier height and a small imaginary frequency corresponding to the reaction coordinate were found for this species. This pitfall of the MPW1K method has been described previously,[49] and in that case, use of a tighter geometry was recommended. In this work, an MP2 calculation was performed on the same transition-state structure, giving a distance that is probably too short (the C–O distance was 2.1 Å) and an excessively high energy barrier to the terminal addition. With the purpose of obtaining a reliable rate constant corresponding to a terminal *ap* addition, the single point CCSD(T)/cc-pVTZ(Q)//MP2/6-31+G(d,p) energy barrier height was lowered 1.5 kcal mol^{-1}, making the order of magnitude of the corresponding rate constant the same as those for the rest of the reactions involved in the MVK+OH system, which are expected to be very similar. This correction is of the same order as the accuracy of the electronic structure method used. Furthermore, the vertical shift of barrier heights to obtain consistent results is a common practice,

 © 2007 Wiley-VCH Verlag GmbH & Co. KGaA, Weinheim

and is necessary especially if we want to build up realistic kinetic models that include effects such as pressure dependence.[50–52] The good agreement between our results and the experimental data validates this small lowering of energy.

The MVK + OH system involves an interesting multichannel, multiwell pressure-dependent reaction. The *ap* pathway starts with OH addition to the terminal carbon atom of the C=C double bond followed by isomerization to an adduct formed by OH addition to the central carbon atom of the same bond. It can be seen that the *ap* pathway matches reaction (S3) described above. Two different wells exist in this pathway, reversibly connected by a transition-state structure corresponding to the isomerization step. A master equation was solved for each well and the corresponding populations obtained. The two equations are coupled through the isomerization channel. The results for two temperatures are summarized in Table 3 and the percentages of the two addition product populations with respect to the total addition product formed are given. These percentages are highly dependent on both temperature and pressure. It can be seen that at a given temperature, the population of the product Padd-c-*ap*1 falls as the pressure rises. On the other hand, at a fixed pressure, the Padd-c-*ap*1 population grows as the temperature rises. The opposite behavior is expected for the product Padd-t-*ap*1, as the percentage is calculated with respect to the total product formed. It can be seen that the excited adduct AB_1* of reaction (S3), in this case Padd-t-*ap*1, requires high pressures to be totally stabilized, and the minimum pressure needed to become collisionally thermalized increases as the temperature rises. This fact can be explained if we consider that the adduct AB_1* is more excited at higher temperatures. As it needs to transfer more energy by collisions, higher pressures are required to stabilize it. On the other hand, the populations in both wells AB_1 and AB_2 of reaction (S3) (Padd-t-*ap*1 and Padd-c-*ap*1 in this case) are connected and cannot be considered independent. The excited AB_1* molecule does not undergo isomerization or dissociation to reactants if it is stabilized by collisions.

Table 3. Percentages of the terminal (Padd-t-*ap*1) and central (Padd-c-*ap*1) addition product populations for *ap* MVK in the 2–100 torr pressure range at 300 and 425 K.

	Product population [%]			
	300 K		425 K	
Pressure [torr]	Padd-t-*ap*1	Padd-c-*ap*1	Padd-t-*ap*1	Padd-c-*ap*1
2	96.3	3.7	70.9	29.1
5	98.2	1.8	79.3	20.7
20	99.3	0.7	88.7	11.3
50	99.7	0.3	93.5	6.5
100	99.7	0.3	95.7	4.3

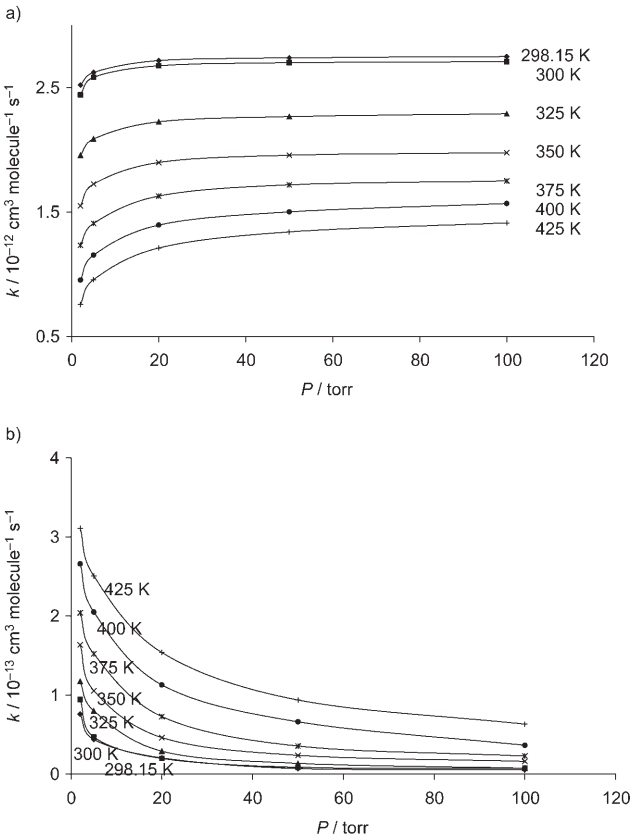

Figure 3. MVK + OH rate constants for a) the add-t-*ap*1 pathway and b) the add-c-*ap*1 pathway versus pressure at different temperatures in helium gas.

The pressure dependence of the rate constant for terminal and central OH addition to *ap* MVK is represented in Figure 3 at different temperatures. The most relevant point to note is that the rate constant for the terminal addition increases as the pressure rises and shows an inverse dependence on temperature, while for the central addition just the opposite behavior is found. It can be seen that the pressure dependence of both reactions increases as the temperature rises.

The *sp* pathways of the MVK + OH system involve two independent processes, namely the terminal and central additions of the OH radical to the C=C double bond. Now, each of these two uncoupled channels corresponds to the simpler reaction (S1) described above in which just one excited adduct, AB*, is formed. The energy barrier height of the terminal addition is lower than the one corresponding to the central addition (−2.2 vs. −1.9 kcal mol^{-1}) and the corresponding rate constants are represented in Figures 4 and 5, respectively. The curves plotted in these figures are analogous to those of the *ap* terminal addition (Figure 3a), showing similar behavior with pressure and temperature variations, and in contrast to those of the *ap* central addition (Figure 3b). As can be seen, the *sp* MVK central addition rate constant shows a stronger variation with pressure than the terminal addition. As an example, at the highest temperature studied, 425 K, the ratio between the rate constants at 100 and 2 torr, k_{100}/k_2, for the central addition is 2.2, while for the terminal addition it is 1.1. The pressure dependence of a recombination reaction like that in reaction (S1) is closely related to the depth of the well corresponding to

 © 2007 Wiley-VCH Verlag GmbH & Co. KGaA, Weinheim

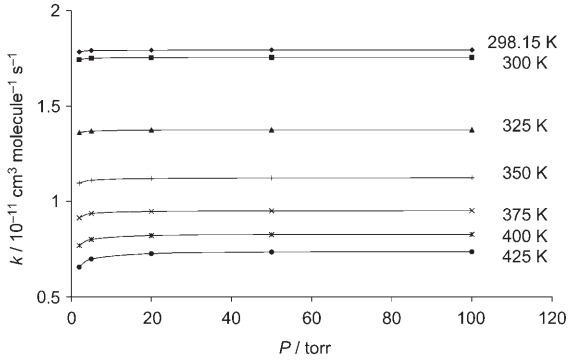

Figure 4. MVK+OH rate constants for the add-t-*sp*1 pathway versus pressure at different temperatures in helium gas.

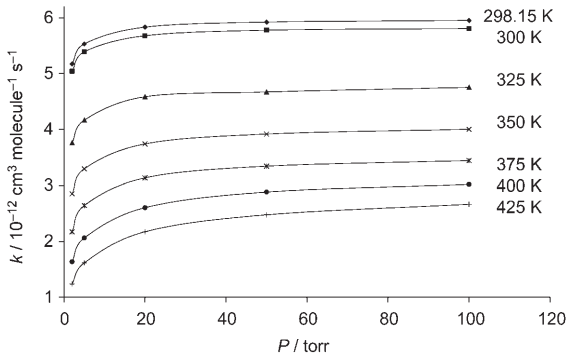

Figure 5. MVK+OH rate constants for the add-c-*sp*1 pathway versus pressure at different temperatures in helium gas.

AB. In the case of OH addition to *sp* MVK, the terminal addition adiabatic reaction energy (classical potential energy plus ZPE) is −31.9 and −26.6 kcal mol^{-1} for the central addition product. The equation for the collision step-size distribution for deactivating collisions used herein is proportional to the exponential of the difference between the initial energy E' and the final energy E after collision, divided by the parameter $\alpha(E')$, as can be seen in Equation (10) of the Computational Methods section. As explained above, $\alpha(E')$ is a linear function of the initial energy E'. In the case of two competitive reactions, R1 and R2, with the same reactants A and B, a hypothetical collisional deactivation from a given energy level E' to another of energy E is pictured in Figure 6. Let us suppose two adducts with the same internal energy, one corresponding to the reaction (R1) and the other participating in reaction (R2). In spite of that, measured relative to the bottom (including the ZPE) of their respective wells (P1 and P2), the energies E_1' and E_2' have different values (that is, the kinetic energies of the two adducts will be different). For instance, let us assume $E_1' > E_2'$. For a deactivating collision that produces a change in energy $\Delta E = E_1' - E_1 = E_2' - E_2$ in Equation (10), the $P(E,E')$ function will be bigger for the reaction with the deeper well, R1, because its $\alpha(E')$ parameter will be larger than the corresponding parameter for reaction (R2). Although the energy of the initial level that is deactivated is the same for both reactions,

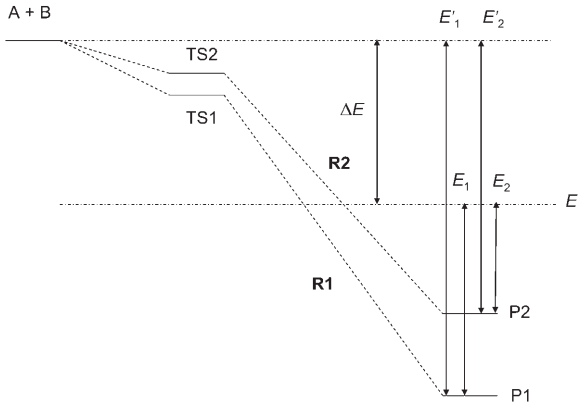

Figure 6. Scheme of a generic reaction with two pathways R1 and R2. A and B are the reactants, TS1 and TS2 are the transition states, and P1 and P2 are the products of the two pathways, respectively. E'_1 and E'_2 are the initial energies of the products, E_1 and E_2 are their final energies, and ΔE is the change of energy produced by deactivating collisions.

the amount of kinetic energy that can be lost by collisions is different. Thus the probability of suffering deactivating collisions is higher for the adduct of reaction (R1), demanding lower pressures in order to stabilize the product P1.

Figure 7 represents the overall rate constant for the MVK+OH system, as defined by Equation (11), in which

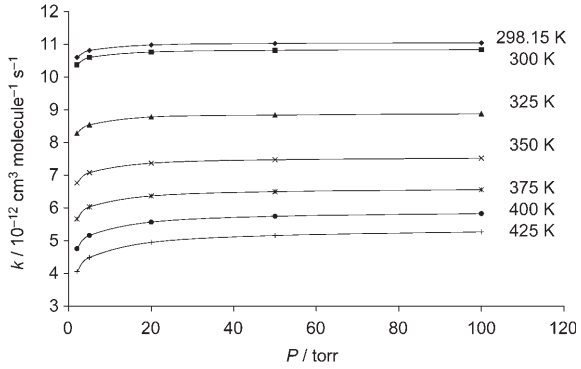

Figure 7. Overall rate constants for the MVK+OH system versus pressure at different temperatures in helium gas.

$k_{i\text{-}j}$ is the rate constant corresponding to the terminal or central addition (i=t or c, respectively) to the *ap* or *sp* conformers (j=*ap* or *sp*, respectively), and *ap* and *sp* refer to the relative population of the two conformers. The MVK+OH overall rate constant is pressure-dependent because all the processes involved depend on pressure. To discuss this pressure dependence of the MVK+OH system, we define a fall-off (i) percentage (that is, the fall-off percentage when the pressure is lowered from i to 2 torr) by Equation (12), where k_i and k_2 are the rate constants at i and 2 torr, respectively. In the case of the MVK+OH system, the fall-off (100) percentage is 4.0% at 298.15 K and 23.0% at 425 K, and the fall-off (5) percentage is 2.0% at 298.15 K and 9.6% at 425 K. From our results we can see that a pressure

 © 2007 Wiley-VCH Verlag GmbH & Co. KGaA, Weinheim

dependence exists for all the temperatures studied in this work, although the lower the temperature, the smaller that pressure dependence.

$$k_{\text{overall}} = (k_{\text{t-}ap} + k_{\text{c-}ap})ap + (k_{\text{t-}sp} + k_{\text{c-}sp})sp \quad (11)$$

$$\text{fall-off } (i) = 100(k_i - k_2)/k_i \quad (12)$$

The theoretical rate constants presented in Figure 7 are in very good agreement with the experimental values. For example, at 300 K and 5 torr, Chuong and Stevens[16] obtained a rate constant of $(1.73 \pm 0.21) \times 10^{-11}$ cm^3 molecule^{-1} s^{-1}, whereas our theoretical rate constant under the same conditions is 1.06×10^{-11} cm^3 molecule^{-1} s^{-1}.

The Arrhenius plots depicted in Figure 8 show a negative dependence of the rate constant on increasing temperatures. This negative activation energy is due to the negative value

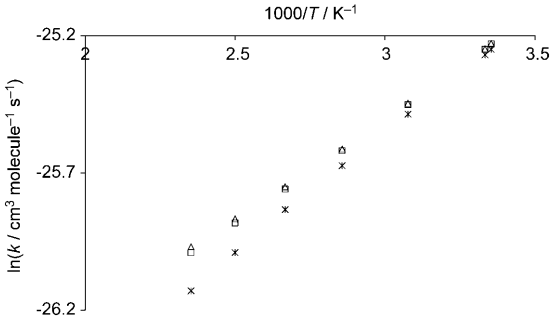

Figure 8. Overall rate constants for the MVK+OH system versus temperature at different pressures (×: 5 torr; □: 50 torr; △: 100 torr).

of the energy barriers of the different reactions that contribute to the overall rate constant in Equation (11). Interestingly, the slopes of the lines in Figure 8 become smaller (energy of activation less negative) as pressure increases owing to the fact that the system is approaching the high-pressure limit. The explanation for this behavior can be rationalized by looking at Figure 7, in which it can be seen that at low pressures, the system is in its fall-off region (i.e., the rate constant is smaller than at higher pressures), and that this fall-off region is larger at higher temperatures. Consequently, the decrease in the rate constants as temperature increases is more pronounced (activation energy becomes more negative) at low pressures than at high pressures.

The slopes of the Arrhenius curves between 298.15 and 425 K for 5, 50, and 100 torr are as follows: $E_a/R = -870$, -759, and -741 K, respectively. Experimentally, values of $E_a/R = -(1170 \pm 80)$ K were found at 5 torr between 300 and 422 K,[16] $E_a/R = -(456 \pm 73)$ K at 50 torr between 298 and 424 K,[19] and $E_a/R = -(612 \pm 49)$ K at 16–100 torr between 232 and 378 K.[15] The experimental slopes are quite well reproduced and the same trends are found, that is, the slopes decrease as the pressure rises.

MACR+OH system: The principal channels of the MACR+OH reactive system are represented in Figure 2. In this reaction only the *ap* conformer was taken into account because the population of the *sp* conformer is negligible at all the temperatures studied, in good agreement with experimental results.[20,53–55]

Determination of the location of the terminal addition transition-state structure of MACR, TSadd-t-*ap*2, is again awkward because the C–O distance between the fragments was found to be too long with MPW1K (3.2 Å) and too short with MP2 (2.1 Å). The same strategy as used for the TSadd-t-*ap*1 species of MVK was applied, the single point CCSD(T)/cc-pVTZ(Q)//MP2/6-31+G(d,p) energy barrier height finally being lowered 1.5 kcal mol^{-1}.

Although the *sp* pathways are not relevant, the MACR+OH system presents a complex multichannel and multiwell profile. The addition of the OH radical to the C=C double bond of MACR is analogous to the reaction of the *ap* conformer in the MVK+OH system. The OH radical adds to the terminal carbon atom to produce an adduct, Padd-t-*ap*2, that can isomerize to the central carbon atom addition product, Padd-c-*ap*2. Again, reaction (S3) can be applied to this pathway and a master equation was solved for each well. A study with the MultiWell program of the variation of Padd-t-*ap*2 and Padd-c-*ap*2 populations with pressure showed that the formation of the latter species is less important than the former. In Table 4 the population percentages of the two addition products are shown. As in the MVK system, it was found that the population of the central adduct falls as the pressure rises. The pressure dependence of the terminal and central addition rate constants is shown in Figure 9, in which the same fall-off behavior as in the MVK *ap* case can be seen.

Table 4. Percentages of the terminal (Padd-t-*ap*2) and central (Padd-c-*ap*2) addition product populations for the *ap* MACR in the 2–100 torr pressure range at 300 and 425 K.

	Product population [%]			
	300 K		425 K	
Pressure [torr]	Padd-t-*ap*2	Padd-c-*ap*2	Padd-t-*ap*2	Padd-c-*ap*2
2	99.0	1.0	87.3	12.7
5	99.7	0.3	92.0	8.0
20	99.8	0.2	96.4	3.6
50	99.9	0.1	97.9	2.1
100	100.0	0.0	98.8	1.2

Unlike the MVK+OH system, the addition of the OH radical to the C=C double bond competes with the hydrogen abstraction of the aldehydic group (-CHO) of MACR. In Figure 2 it is seen that the barrier height for the abstraction is 1.1 kcal mol^{-1} less than that for the terminal addition. In the abstraction pathway, an adduct is formed between the radical product and a water molecule, PCabs-*ap*2, which can irreversibly dissociate to the products, Pabs-*ap*2 and H_2O, or revert to the reactants. This pathway corresponds to reaction (S2) described above. In this case, the dissociation of PCabs-*ap*2 has no energy barrier and the separate products

 © 2007 Wiley-VCH Verlag GmbH & Co. KGaA, Weinheim

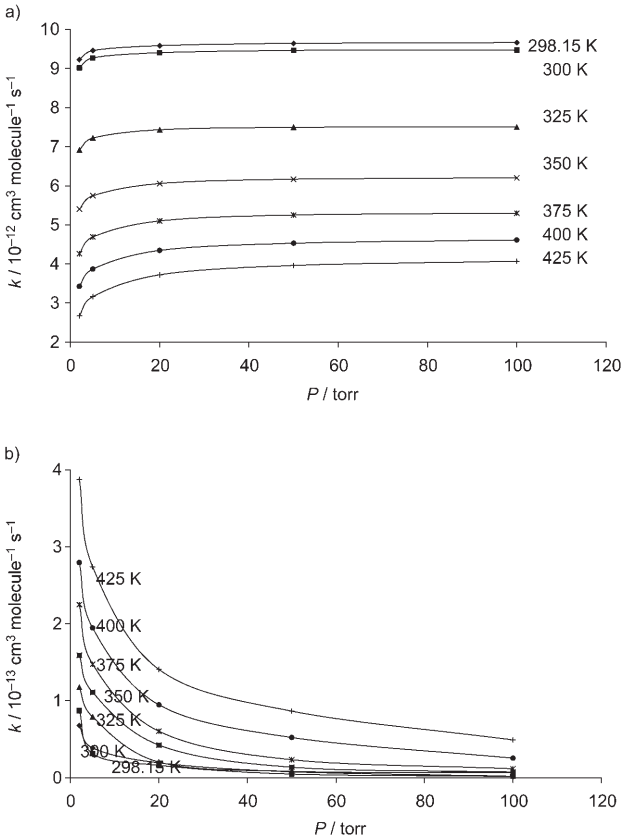

Figure 9. MACR+OH rate constants for a) the add-t-*ap*2 pathway and b) the add-c-*ap*2 pathway versus pressure at different temperatures in helium gas.

are only 2.9 kcal mol^{-1} less stable. So it is expected that when the adduct PCabs-*ap*2 is formed, it immediately suffers irreversible dissociation into products. This fact makes the abstraction reaction independent of pressure, as confirmed by our MultiWell calculation of the populations of the different species as a function of pressure, showing that the separate products are 100% populated at all pressures. The data in Table 5 show the variation in the MACR abstraction rate constant with temperature. The rate constant decreases with increasing temperature and so the activation energy corresponding to this process is negative, again due to the negative value of the energy barrier.

Variation with pressure of the overall rate constants as a sum of the abstraction, terminal addition, and central addition rates of the MACR+OH system, given by Equation (13), is represented in Figure 10. The addition reactions determine the pressure-dependence reflected in Figure 10, as the abstraction rate constant is the same at all pressures.

Table 5. Rate constants for the MACR abstraction channel versus temperature.

T [K]	$k_{\text{abs-}ap2}$ [10^{-11} cm^3 molecule^{-1} s^{-1}]
298.15	1.7
300	1.7
325	1.5
350	1.3
375	1.2
400	1.2
425	1.1

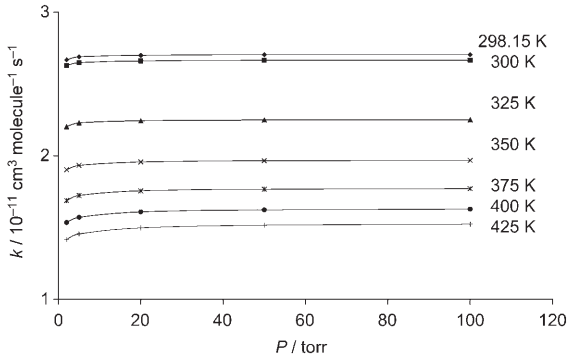

Figure 10. Overall rate constants for the MACR+OH system versus pressure at different temperatures in helium gas.

Although a slight pressure dependence is observed, this is less important than in the MVK+OH system. This can be checked by comparing the fall-off (*i*) percentages [Equation (12)]. For the MACR+OH system, the fall-off (100) percentage is 1.4% at 298.15 K and 6.9% at 425 K, whilst the fall-off (5) percentage is 0.8% at 298.15 K and 2.6% at 425 K. These values are clearly smaller than those of the MVK+OH system, confirming that the pressure-dependence is much less important.

$$k_{\text{overall}} = k_{\text{t-}ap} + k_{\text{c-}ap} + k_{\text{abs-}ap} \quad (13)$$

Again the theoretical rate constants are very similar to the experimental values. As an example, the rate constant experimentally obtained at 300 K and 5 torr by Chuong and Stevens[16] is $(3.23 \pm 0.36) \times 10^{-11}$ cm^3 molecule^{-1} s^{-1} and our theoretical value is 2.65×10^{-11} cm^3 molecule^{-1} s^{-1}, showing very good agreement.

Arrhenius plots of the rate constants are shown in Figure 11. It can be observed that, again, the activation energy is negative, as in the MVK+OH system. On the other hand, it can also be seen that the variation of the over-

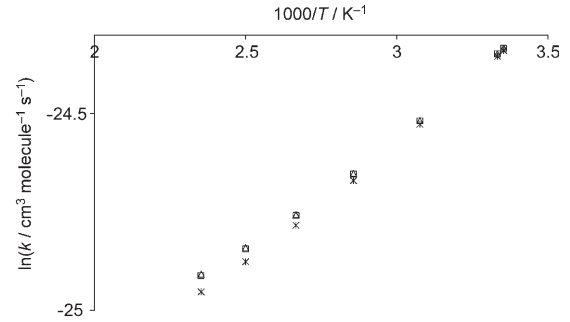

Figure 11. Overall rate constants for the MACR+OH system versus temperature at different pressures (×: 5 torr; □: 50 torr; △: 100 torr).

 © 2007 Wiley-VCH Verlag GmbH & Co. KGaA, Weinheim

all rate constant with temperature slightly depends on the pressure. This is due to the addition processes, as the abstraction rate constant does not vary with pressure. This result agrees well with the experimental Arrhenius plots for the MACR + OH system. The slopes of our theoretical Arrhenius curves between 298.15 and 425 K for pressures of 5, 50, and 100 torr are as follows: $E_a/R = -619$, -585, and -580 K, respectively. The experimental values are $E_a/R = -(1050\pm120)$ K at 5 torr and between 300 and 422 K,[16] $E_a/R = -(175\pm52)$ K at 50 torr and between 300 and 423 K,[19] and $E_a/R = -(379\pm46)$ K at 20–100 torr[15] and between 234 and 373 K. Again, the experimental slopes are quite well reproduced, and the same trend is found, that is, the slopes decrease as the pressure rises, although the pressure effect is less than for the MVK case.

Conclusion

The main pathways involved in the multiwell, multichannel methyl vinyl ketone + OH and methacrolein + OH systems have been studied by means of high-level electronic structure calculations. The corresponding microcanonical rate constants were obtained and conveniently used, along with the collisional energy transfer model, to establish the master equation that describes the variation of the rate constant with pressure. The solution of the master equation has shown the dependency of the rate constants on temperature and pressure. We have shown that the combined pressure and temperature dependence of each reaction is a consequence of the subtle balance between the OH additions at the high-pressure limit, the OH additions at the low-pressure fall-off region, and the pressure-independent hydrogen abstraction reaction. In particular, we have found that the fall-off region of the OH additions contributes to the inverse temperature dependence of the rate constants in the Arrhenius plots, leading to pressure-dependent negative activation energies. The pressure dependence of the methyl vinyl ketone + OH reaction is clearly more important than in the methacrolein + OH reaction as a result of the weight of the hydrogen-abstraction process in this second system. Other interesting aspects of these reactions that have been reflected in our study are the pressure dependence of the population of the different species in a multiwell pathway and the influence of the well depth in the deactivation collisional process. In all, the agreement between our theoretical rate constants (and their pressure and temperature dependence) and the corresponding experimental measurements turns out to be quite good, especially taking into account the number of factors that determine the behavior of these quite challenging reactions.

The combined pressure and temperature dependence of gas-phase reactions, such as atmospheric reactions, is becoming more widely studied, and their theoretical determination by means of master equations will probably become a commonplace in the future. In this paper we have presented two illustrative examples for which a complete description at different pressures and temperatures is needed in order to correctly interpret the complex behavior of the overall reactions.

Acknowledgements

The authors are grateful for financial support from the Ministerio de Educación y Ciencia and the Fondo Europeo de Desarrollo Regional through projects CTQ2005-07115/BQU and CTQ2004-07768-C02-01, from the DURSI de la Generalitat de Catalunya (2005SGR00400), and from the DGEUI of Generalitat Valenciana through projects GRUPOS03/173 and INF01-51. Use of the computational facilities at the Centre de Supercomputació de Catalunya is also acknowledged. M.O.-P. acknowledges the Spanish MEC for an FPU grant. We would also like to acknowledge Professor J. R. Barker for providing us with the MultiWell code and for his assistance.

[1] B. J. Finlayson-Pitts, J. N. Pitts, *Science* **1997**, *276*, 1045.
[2] A. R. Ravishankara, *Chem. Rev.* **2003**, *103*, 4505.
[3] G. Brasseur, J. J. Orlando, G. S. Tyndall, *Atmospheric Chemistry and Global Change*, Oxford University Press, New York, **2000**.
[4] R. P. Wayne, *Chemistry of Atmospheres: An Introduction to the Chemistry of the Atmospheres of Earth, the Planets, and Their Satellites*, 3rd ed., Oxford University Press, New York, **2000**.
[5] E. Pollak, P. Talkner, *Chaos* **2005**, *15*, 026116.
[6] D. G. Truhlar, A. D. Isaacson, B. C. Garrett in *Theory of Chemical Reaction Dynamics, Vol. 4* (Ed.: M. Baer), CRC Press, Boca Raton, Florida, **1985**, p. 65.
[7] J. R. Barker, D. M. Golden, *Chem. Rev.* **2003**, *103*, 4577.
[8] R. G. Gilbert, S. C. Smith, *Theory of Unimolecular and Recombination Reactions*, Blackwell Scientific, Oxford, **1990**.
[9] UNIMOL Program Suite, R. G. Gilbert, M. J. T. Jordan, S. C. Smith, School of Chemistry, Sydney (Australia), **1990**.
[10] VariFlex Software, version 1.0, S. J. Klippenstein, A. F. Wagner, S. H. Robertson, R. Dunbar, D. M. Wardlaw, Argonne National Laboratory, **1999**.
[11] ChemRate. A Calculational Data Base for Unimolecular Reactions, V. Mokrushin, W. Tsang, National Institute of Standards and Technology, Gaithersburg, MD, **2000**.
[12] S. C. Smith, E. W.-G. Diau, H. W. Schranz, *UNIRATE, Energy and Angular Momentum Resolved Generalized Transition State Theory Fortran Code*, **2001**.
[13] T. Baer, W. L. Hase, *Unimolecular Reaction Dynamics*, Oxford University Press, New York, **1996**.
[14] a) E. C. Tuazon, R. Atkinson, *Int. J. Chem. Kinet.* **1989**, *21*, 1141; b) E. C. Tuazon, R. Atkinson, *Int. J. Chem. Kinet.* **1990**, *22*, 591.
[15] T. Gierczak, J. B. Burkholder, R. K. Talukdar, A. Mellouki, S. B. Barone, A. R. Ravishankara, *J. Photochem. Photobiol. A* **1997**, *110*, 1.
[16] B. Chuong, P. S. Stevens, *J. Phys. Chem. A* **2003**, *107*, 2185.
[17] B. Chuong, P. S. Stevens, *Int. J. Chem. Kinet.* **2004**, *36*, 12.
[18] A. L. Holloway, J. Treacy, H. Sidebottom, A. Mellouki, V. Daele, G. Le Bras, I. Barnes, *J. Photochem. Photobiol. A* **2005**, *176*, 183.
[19] T. E. Kleindienst, G. W. Harris, J. N. Pitts, *Environ. Sci. Technol.* **1982**, *16*, 844.
[20] M. Ochando-Pardo, I. Nebot-Gil, À. González-Lafont, J. M. Lluch, *ChemPhysChem* **2005**, *6*, 1567.
[21] B. J. Lynch, P. L. Fast, M. Harris, D. G. Truhlar, *J. Phys. Chem. A* **2000**, *104*, 4811.
[22] B. J. Lynch, D. G. Truhlar, *J. Phys. Chem. A* **2001**, *105*, 2936.
[23] Y. Zhao, D. G. Truhlar, *J. Phys. Chem. A* **2004**, *108*, 6908.
[24] Y. Zhao, D. G. Truhlar, *J. Phys. Chem. A* **2005**, *109*, 5656.
[25] F. Jensen, *Chem. Phys. Lett.* **1990**, *169*, 519.
[26] J. Villà, D. G. Truhlar, *Theor. Chem. Acc.* **1997**, *97*, 317.
[27] À. González-Lafont, J. Villà, J. M. Lluch, J. Bertran, R. Steckler, D. G. Truhlar, *J. Phys. Chem. A* **1998**, *102*, 3420.

 © 2007 Wiley-VCH Verlag GmbH & Co. KGaA, Weinheim

[28] Y. Y. Chuang, E. L. Coitiño, D. G. Truhlar, *J. Phys. Chem. A* **2000**, *104*, 446.
[29] J. F. Stanton, *J. Chem. Phys.* **1994**, *101*, 371.
[30] P. J. Knowles, C. Hampel, H. J. Werner, *J. Chem. Phys.* **1993**, *99*, 5219.
[31] K. A. Peterson, T. H. Dunning, *J. Phys. Chem. A* **1997**, *101*, 6280.
[32] M. Rittby, R. J. Bartlett, *J. Phys. Chem.* **1988**, *92*, 3033.
[33] a) G. E. Scuseria, *Chem. Phys. Lett.* **1991**, *176*, 27; b) W. F. Lei, A. Derecskei-Kovacs, R. Y. Zhang, *J. Chem. Phys.* **2000**, *113*, 5354.
[34] Gaussian 03, Revision C.02, M. J. Frisch, G. W. Trucks, H. B. Schlegel, G. E. Scuseria, M. A. Robb, J. R. Cheeseman, J. A. Montgomery, Jr., T. Vreven, K. N. Kudin, J. C. Burant, J. M. Millam, S. S. Iyengar, J. Tomasi, V. Barone, B. Mennucci, M. Cossi, G. Scalmani, N. Rega, G. A. Petersson, H. Nakatsuji, M. Hada, M. Ehara, K. Toyota, R. Fukuda, J. Hasegawa, M. Ishida, T. Nakajima, Y. Honda, O. Kitao, H. Nakai, M. Klene, X. Li, J. E. Knox, H. P. Hratchian, J. B. Cross, V. Bakken, C. Adamo, J. Jaramillo, R. Gomperts, R. E. Stratmann, O. Yazyev, A. J. Austin, R. Cammi, C. Pomelli, J. W. Ochterski, P. Y. Ayala, K. Morokuma, G. A. Voth, P. Salvador, J. J. Dannenberg, V. G. Zakrzewski, S. Dapprich, A. D. Daniels, M. C. Strain, O. Farkas, D. K. Malick, A. D. Rabuck, K. Raghavachari, J. B. Foresman, J. V. Ortiz, Q. Cui, A. G. Baboul, S. Clifford, J. Cioslowski, B. B. Stefanov, G. Liu, A. Liashenko, P. Piskorz, I. Komaromi, R. L. Martin, D. J. Fox, T. Keith, M. A. Al-Laham, C. Y. Peng, A. Nanayakkara, M. Challacombe, P. M. W. Gill, B. Johnson, W. Chen, M. W. Wong, C. Gonzalez, J. A. Pople, Gaussian, Inc., Wallingford CT, **2004**.
[35] MOLPRO (version 2002.6), H.-J. Werner, P. J. Knowles, M. Schütz, R. Lindh, P. Celani, T. Korona, G. Rauhut, F. R. Manby, R. D. Amos, A. Bernhardsson, A. Berning, D. L. Cooper, M. J. O. Deegan, A. J. Dobbyn, F. Eckert, C. Hampel, G. Hetzer, A. W. Lloyd, S. J. McNicholas, W. Meyer, M. E. Mura, A. Nicklaß, P. Palmieri, R. Pitzer, U. Schumann, H. Stoll, A. J. Stone, R. Tarroni, T. Thorsteinsson, Birmingham (UK), **2003**.
[36] MultiWell Program Suite (version 1.4.1), J. R. Barker, N. F. Ortiz, J. M. Preses, L. L. Lohr, University of Michigan, Ann Arbor, MI, **2004**.
[37] J. R. Barker, *Int. J. Chem. Kinet.* **2001**, *33*, 232.
[38] D. M. Golden, J. R. Barker, L. L. Lohr, *J. Phys. Chem. A* **2003**, *107*, 11057.
[39] J. Villà, J. C. Corchado, À. González-Lafont, J. M. Lluch, D. G. Truhlar, *J. Phys. Chem. A* **1999**, *103*, 5061.
[40] S. E. Stein, B. S. Rabinovitch, *J. Chem. Phys.* **1973**, *58*, 2438.
[41] W. Forst, *Theory of Unimolecular Reactions*, Academic Press, New York, London, **1973**.
[42] K. A. Holbrook, S. H. Robertson, P. J. Robinson, M. J. Pilling, *Unimolecular Reactions*, 2nd ed., Wiley, Chichester, **1996**.
[43] E. A. Halkiadakis, R. G. Bowrey, *Chem. Eng. Sci.* **1975**, *30*, 53.
[44] F. M. Mourits, F. H. A. Rummens, *Can. J. Chem.* **1977**, *55*, 3007.
[45] L. I. Stiel, G. Thodos, *J. Chem. Eng. Data* **1962**, *7*, 234.
[46] *Perry's Chemical Engineer's Handbook* (Eds.: D. W. Green, J. O. Maloney), 6th ed., McGraw-Hill, New York, **1984**.
[47] T. Lenzer, K. Luther, K. Reihs, A. C. Symonds, *J. Chem. Phys.* **2000**, *112*, 4090.
[48] J. Desmedt, F. Vanhouteghem, C. Vanalsenoy, H. J. Geise, B. Vanderveken, P. Coppens, *J. Mol. Struct.* **1989**, *195*, 227.
[49] M. Saeys, M. F. Reyniers, G. B. Marin, V. Van Speybroeck, M. Waroquier, *J. Phys. Chem. A* **2003**, *107*, 9147.
[50] W. C. Chen, R. A. Marcus, *J. Chem. Phys.* **2005**, *123*, 094307.
[51] Y. M. Choi, M. C. Lin, *ChemPhysChem* **2004**, *5*, 225.
[52] J. P. Senosiain, S. J. Klippenstein, J. A. Miller, *J. Phys. Chem. A* **2005**, *109*, 6045.
[53] J. R. Durig, J. Qiu, B. Dehoff, T. S. Little, *Spectrochim. Acta, Part A* **1986**, *42*, 89.
[54] M. Suzuki, K. Kozima, *J. Mol. Spectrosc.* **1971**, *38*, 314.
[55] Y. Wang, J. Desmedt, I. Coucke, C. Vanalsenoy, H. J. Geise, *J. Mol. Struct.* **1993**, *299*, 43.

Received: April 13, 2006
Published online: October 26, 2006

 © 2007 Wiley-VCH Verlag GmbH & Co. KGaA, Weinheim